

FocalCount: Towards Class-Count Imbalance in Class-Agnostic Counting

Huilin Zhu^{1,2}, Jingling Yuan^{1,*}, Zhengwei Yang³, Yu Guo^{4,2}, Xian Zhong^{1,*}, Shengfeng He²
¹ Hubei Key Laboratory of Transportation Internet of Things, Wuhan University of Technology
² School of Computing and Information Systems, Singapore Management University
³ School of Computer Science, Wuhan University
⁴ School of Navigation, Wuhan University of Technology
 yjl@whut.edu.cn, zhongx@whut.edu.cn

Abstract

In class-agnostic object counting, the goal is to estimate the total number of object instances in an image without distinguishing between specific categories. Existing methods often predict this count without considering class-specific outputs, leading to inaccuracies when such outputs are required. These inaccuracies stem from two key challenges: 1) the prevalence of single-category images in datasets, which leads models to generalize specific categories as representative of all objects, and 2) the use of mean squared error loss during training, which applies uniform penalization. This uniform penalty disregards errors in less frequent categories, particularly when these errors contribute minimally to the overall loss. To address these issues, we propose FocalCount, a novel approach that leverages diverse feature attributes to estimate the number of object categories in an image. This estimate serves as a weighted factor to correct class-count imbalances. Additionally, we introduce Focal-MSE, a new loss function that integrates binary cross-entropy to generate stronger error gradients, enhancing the model’s sensitivity to errors in underrepresented categories. Our approach significantly improves the model’s ability to distinguish between specific classes and general counts, demonstrating superior performance and scalability in both few-shot and zero-shot scenarios across three object counting datasets. The code will be released soon.

1. Introduction

Object counting is a fundamental task in computer vision, involving the estimation of object quantities in images or videos. Traditionally, this task has focused on specific categories, such as crowds, vehicles, and cells [2, 19, 25, 27]. However, these methods are limited by their reliance on predefined categories and specific training datasets, which restrict their generalizability. To address this, class-agnostic

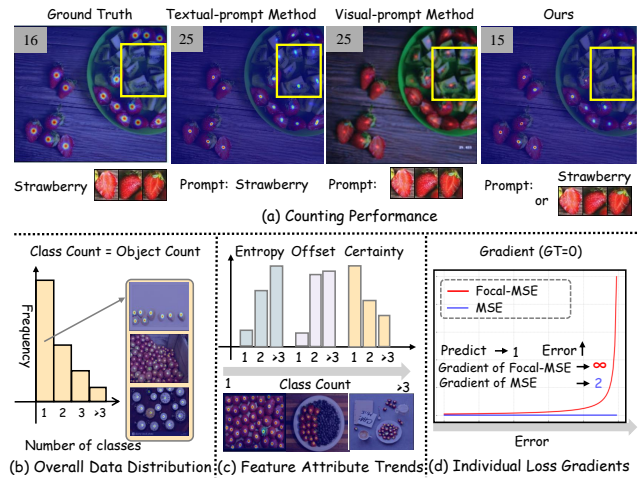


Figure 1. **Illustration of Object Counting.** (a) Miscounting of unspecified classes by CounTR (few-shot visual prompt) and CLIP-Count (zero-shot textual prompt). (b) Object count distribution showing single-category dominance in FSC-147. (c) Impact of category diversity on counting accuracy using feature attributes. (d) Gradient comparison between Focal-MSE and MSE.

object counting, operating independently of predefined categories, has gained significant attention for its broader applicability. Class-agnostic object counting methods can be categorized into three main types: visual-prompt-based, textual-prompt-based, and reference-less. Visual-prompt methods perform well using image references but require bounding box annotations during inference. Textual-prompt methods allow category specification without bounding boxes but struggle due to the semantic gap between text and images, making category association challenging. Reference-less methods minimize annotation requirements but do not permit category specification, often resulting in the counting of all visible objects, which may not align with specific objectives.

To enhance category-specific counting, we conduct an

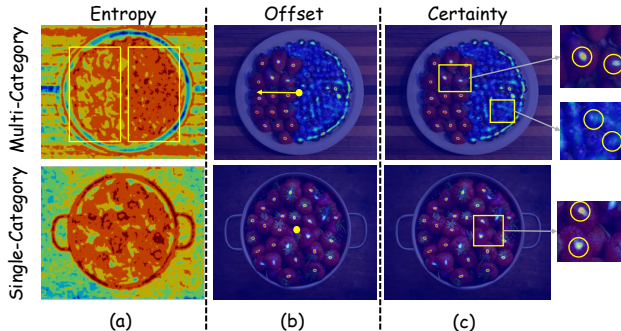


Figure 2. **Illustration of Feature Attributes in Single-Category versus Multi-Category Images.**

extensive analysis of textual-prompt and visual-prompt methods, revealing key insights. As shown in Fig. 1(a), these methods often count all objects in an image, regardless of prompts, resembling the behavior of reference-less methods and undermining precise object counting. Further analysis indicates that model bias contributes significantly to this issue. As illustrated in Fig. 1(b), many images in object counting datasets contain only one category, with the total object count matching the specified category. This imbalance causes models to indiscriminately count all objects, exacerbating the problem. Additionally, Fig. 1(d) shows that MSE loss, the most commonly used loss function in object counting, penalizes large and small prediction errors equally. In datasets with few multi-category images, this loss function fails to address small counts of non-specified categories effectively.

To address indiscriminate object counting, two key objectives must be met: mitigating data imbalances by increasing focus on multi-category images, and implementing a loss function that enhances sensitivity to errors in regions with non-specified classes, thereby improving supervision. A common strategy for handling data imbalance is reweighting [7, 21, 24], which assigns higher weights to minority samples. However, in class-agnostic counting, each image is labeled with only one category, making it difficult to infer the number of categories based solely on class labels. Despite this, the number of categories within an image can be inferred. As shown in Fig. 1(c), there is a correlation between discernible patterns in feature attributes and the number of categories in images.

Moreover, as shown in Fig. 2, distinct differences in feature attributes are observed between multi-category and single-category images. Specifically, Fig. 2(a) shows that images with multiple categories exhibit higher entropy, reflecting greater information complexity. In contrast, single-category images typically display a more centralized specified category, while multi-category images show an offset in the specified category area, as depicted in Fig. 2(b). In-

terestingly, although objects from non-specified categories are counted, their certainty is significantly lower than that of specified categories, as shown in Fig. 2(c).

These insights led to the development of FocalCount, a method that assigns different weights to data based on the likelihood of containing multiple categories. Additionally, as shown in Fig. 1(d), while Focal-MSE provides more adaptive gradients for reducing errors in localized regions compared to MSE, it alone lacks the precision required for exact quantity supervision. To address this, we integrate Focal-MSE into a curriculum learning framework, where it is used in the early stages of training alongside error-sensitive entropy. This approach improves precise quantity supervision and enhances the model’s sensitivity to errors in non-specified categories.

In summary, our contributions are fourfold:

- We are the first to identify that the prevalent data imbalance, where single-category images dominate in object counting datasets, leads most methods to count all objects in an image rather than focusing on the specified category.
- We propose FocalCount, a novel method that addresses data imbalance by estimating image category counts through the relation between feature attributes and the number of categories.
- We introduce Focal-MSE loss, a new loss function that integrates binary cross-entropy to modulate training with stronger error gradients, enhancing the model’s sensitivity to errors in non-specified categories.
- Extensive experiments on three object counting datasets in both few-shot and zero-shot settings demonstrate the state-of-the-art accuracy and generalizability of FocalCount.

2. Related Work

2.1. Object Counting

Object counting plays a crucial role in applications such as public safety, administration, and labor efficiency. Traditional methods [23, 26, 31, 32] are restricted to fixed categories and require retraining when new categories are introduced. In contrast, class-agnostic counting [4, 6, 14, 18, 20] offers more flexible solutions, supporting scenarios with limited data and enabling few-shot, reference-less, and zero-shot counting methods.

Few-shot object counting addresses scenarios with limited annotated data. GMN [18] formulates class-agnostic counting as a matching task, leading to FamNet [22], which incorporates ROI Pooling. BMNet [26] introduces a bilinear matching network to refine similarity assessments. LOCA [3] enhances feature representation and exemplar adaptation, while CounTR [16] uses transformers to scale counting tasks. CACViT [29] integrates Vision Transformers (ViT) into object counting for improved performance.

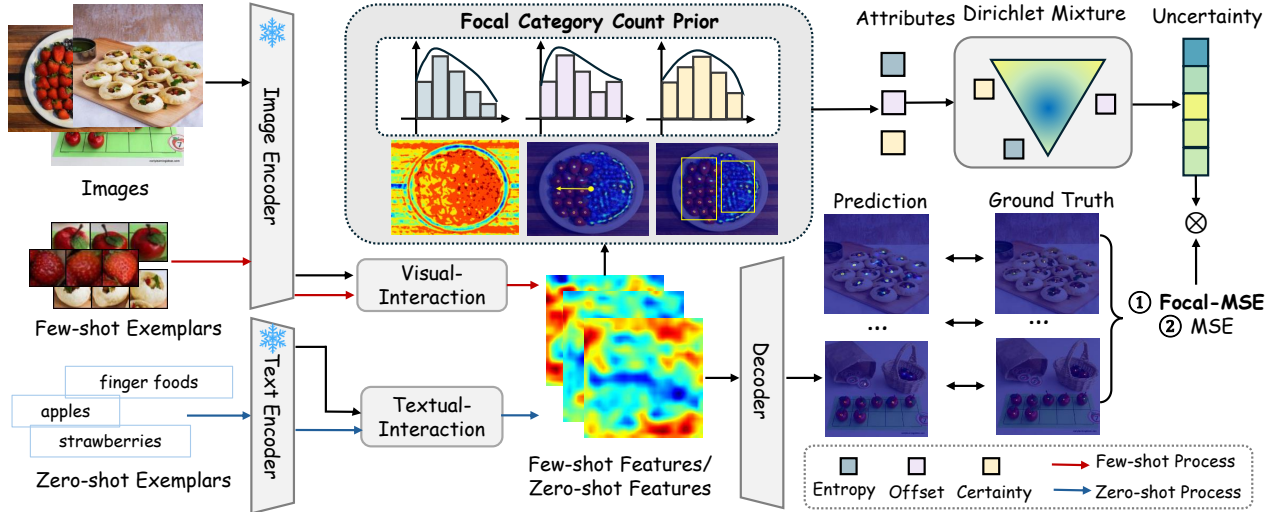


Figure 3. **Overview of the FocalCount Method.** (1) Mitigating data imbalance by estimating the Focal Category Count Prior using entropy, offset, and feature certainty. (2) Employing dual-phase curriculum learning: initially applying Focal-MSE to enhance quantity supervision and sensitivity to errors in unspecified categories, followed by MSE for precise learning.

Zero-shot object counting operates without the need for category-specific training data. CLIP-Count [11] leverages CLIP to encode text and images separately, enabling semantic associations, while VLCount [12] enhances text-image association learning. PseCo [10] introduces a SAM-based framework for segmentation, dot mapping, and detection, offering broad applicability but requiring significant computational resources.

Reference-less object counting do not rely on specific references. ZSC [30] generates prototypes using textual inputs and filters image patches, reducing labeling requirements but facing scalability challenges. While these methods are flexible and scalable, they often struggle with accuracy across diverse categories due to the absence of multi-category density map labels in most datasets.

2.2. Counting Loss

The most commonly used loss function in object counting is mean squared error (MSE) loss [22], which effectively measures the difference between predicted and ground truth maps. To capture associations, GMN [18] introduces a similarity loss that quantifies the relations between predicted and actual similarities, while FamNet [22] incorporates a perturbation loss to increase robustness. LOCA [3] adds an auxiliary loss to support multi-channel learning. Other methods [10, 11] employ an InfoNCE-based contrastive loss [28] to distinguish target regions from the background, while VA-Count [34] uses contrastive loss to differentiate between known and unknown classes.

However, these loss functions do not address the imbalance between single-label and multi-label data, which of-

ten leads models to indiscriminately count all objects. Inspired by Focal Loss [15], we propose Focal-MSE, an error-sensitive loss function that enhances sensitivity to specific regions. Focal-MSE promotes intra-class compactness and inter-class distinctiveness, transforming counting into a probability metric for specified categories and ensuring precise counting while overcoming the limitations of traditional loss.

3. Proposed Method

3.1. Problem Definition

Class-agnostic object counting models often suffer from a bias towards single-category images due to dataset imbalances, resulting in inaccurate object counts that fail to focus on specified categories. We propose FocalCount, a novel method to address this data imbalance and improve model sensitivity to errors. As illustrated in Fig. 3, FocalCount first analyzes feature attribute trends to emphasize images with multiple categories (See Sec. 3.2). Then, we apply Focal-MSE, an error-sensitive loss function, to improve accuracy in detecting density map errors, particularly for unspecified categories in multi-category images (See Sec. 3.4).

Let the training set of images be denoted as $\{I_i\}_{i=0}^n$, and the exemplars (either visual or textual prompts) as $\{P_i\}_{i=0}^n$. The output features are represented as $\{F_i\}_{i=0}^n$, the predicted density maps as $\{M_i^p\}_{i=0}^n$, and the ground truth density maps as $\{M_i^g\}_{i=0}^n$. The objective is to minimize the following loss function, where U_i denotes data adjustment weights, \mathcal{L} is the loss function, and n is the number of images:

$$\text{Objective} = \min \sum_{i=0}^n U_i \mathcal{L}(M_i^p, M_i^g). \quad (1)$$

3.2. Focal Imbalance Rectification

3.2.1 Focal Category Count Prior.

In object counting datasets, images often contain only a single category, making it challenging to estimate the number of categories from labels alone. However, the presence of multiple categories can leave identifiable traces. By analyzing feature attributes, we can infer the likelihood of multiple categories. Fig. 4 shows the relation between category count and three attributes: entropy and offset, which are positively correlated with category count, and certainty, which is negatively correlated. Combining these attributes improves the reliability of category count estimation.

3.2.2 Feature Extraction.

Given a batch of images $\{I_i\}_{i=1}^n$ and exemplars $\{P_i\}_{i=1}^n$, we input them into the encoder $\phi(\cdot)$ to obtain features $\{F_i\}_{i=1}^n$:

$$F_i = \phi(I_i, P_i). \quad (2)$$

Entropy Calculation. Entropy, which measures feature complexity, generally increases with the amount of information in an image and is positively correlated with the number of categories. It is computed as follows:

$$E_i = -\sum_{h=1}^H \sum_{w=1}^W \sum_{c=1}^C [F_i \log F_i + (1 - F_i) \log(1 - F_i)], \quad (3)$$

where E_i represents the entropy across the feature dimensions: H for height, W for width, and C for channels.

Offset Calculation. The feature offset measures the spatial deviation of activations from the image’s geometric center, indicating the distribution of features. Offset is positively correlated with category count; objects in single-category images are more centrally located, with centralization decreasing as category diversity increases:

$$O_i = \left| \frac{\sum_{h=1}^H \sum_{w=1}^W w F_i}{\sum_{h=1}^H \sum_{w=1}^W F_i} - \frac{W}{2} \right|, \quad (4)$$

where O_i reflects the x-axis deviation of the centroid from the image center for each feature map F_i .

Certainty Calculation. Certainty measures the confidence in predictions and is negatively correlated with category count. The model exhibits lower confidence in areas with unspecified categories. Certainty C_i is derived by applying a sigmoid function to the normalized mean magnitude of activations μ_i , as follows:

$$S_i = \sum_{h=1}^H \sum_{w=1}^W |F_{i,h,w}|, \quad \mu_i = \frac{S_i}{H \times W}, \quad (5)$$

where S_i is the sum of absolute activations in the i -th feature map, and μ_i represents the normalized mean magnitude of

activations. Finally, feature certainty C_i is computed by applying a sigmoid function to μ_i , followed by inversion:

$$C_i = 1 - \text{sigmoid}(\mu_i). \quad (6)$$

3.3. Dirichlet Mixture

Although entropy, offset, and certainty correlate with category count, these relations are not absolute. To achieve a more reliable evaluation, we combine these attributes into a composite weight using the Dirichlet distribution. Given attributes E_i (entropy), O_i (offset), and C_i (certainty), the Dirichlet distribution is parameterized by a concentration vector $\alpha = [\alpha_1, \alpha_2, \alpha_3]$:

$$p(w | \alpha) = \frac{1}{B(\alpha)} \prod_{k=1}^3 w_k^{\alpha_k - 1}, \quad (7)$$

where $w = [w_1, w_2, w_3]$ is the weight vector with $\sum_{k=1}^3 w_k = 1$, and $B(\alpha)$ is the multivariate beta function:

$$B(\alpha) = \frac{\prod_{k=1}^3 \Gamma(\alpha_k)}{\Gamma(\sum_{k=1}^3 \alpha_k)}. \quad (8)$$

Sampling from the Dirichlet distribution:

$$w \sim \text{Dirichlet}(\alpha), \quad (9)$$

where the sampled weight vector w combines the attributes into a weighted representation:

$$U_C = \sum_{k=1}^3 w_k U_k, \quad (10)$$

where $U_1 = E_i$, $U_2 = O_i$, and $U_3 = C_i$. The final U_C represents the combined certainty of the three attributes.

3.4. Error-Sensitive Focal-MSE

To enhance model sensitivity to target regions and improve accuracy in object counting, we introduce Focal-MSE, a novel loss function that modifies traditional MSE loss. The predicted density map M^P and ground truth map M_i^g are treated as matrices, where each entry in M_i^g indicates object presence, and M^P represents the predicted probability. Focal-MSE focuses on sparsely populated and error-prone areas to ensure precise counting. The error-sensitive (ES) loss is computed as:

$$\mathcal{L}_i^{\text{ES}}(M_i^P, M_i^g) = -\sum_{h=1}^H \sum_{w=1}^W \left[M_i^g \log(M_i^P) + (1 - M_i^g) \log(1 - M_i^P) \right]. \quad (11)$$

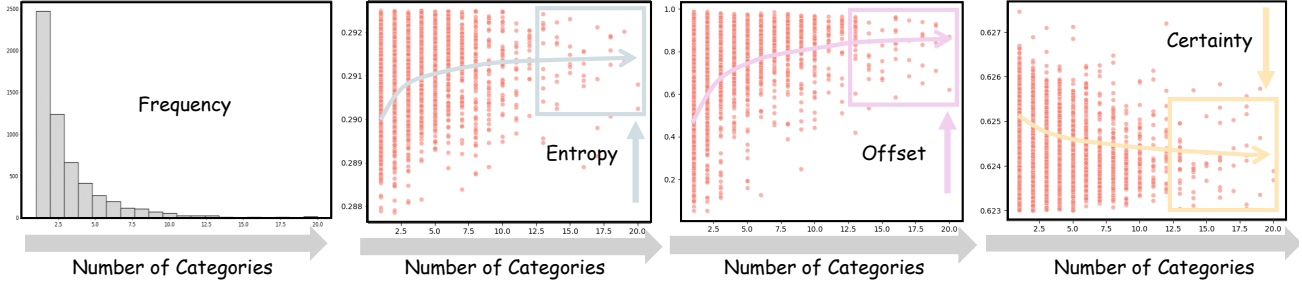


Figure 4. **Relation between Number of Categories and Attributes in PASCAL VOC [5].** As the number of categories increases, entropy and offset rise, while certainty declines, indicating greater complexity.

The Focal-MSE loss, combining MSE loss with ES loss, is defined as:

$$\mathcal{L}_i^{\text{FMSE}}(M_i^p, M_i^g) = \sum_{h=1}^H \sum_{w=1}^W (M_i^p - M_i^g)^2 + \mathcal{L}_i^{\text{ES}}. \quad (12)$$

Focal-MSE enhances category information, although it may not yield precise density maps for object counting. MSE loss is therefore introduced in the second phase to ensure accuracy:

$$\mathcal{L}_i^{\text{MSE}}(M_i^p, M_i^g) = - \sum_{h=1}^H \sum_{w=1}^W (M_i^p - M_i^g)^2. \quad (13)$$

Dual-phase Curriculum Loss. FocalCount employs a curriculum learning scheme for enhanced supervision and sensitivity to non-specified category errors, using a dual-phase loss. Focal-MSE is effective in early training stages with ambiguous information, while MSE loss is prioritized later to refine predictions. Assuming t epochs for the first phase, the dual-phase loss function is:

$$\mathcal{L}_i^D = \begin{cases} \mathcal{L}_i^{\text{FMSE}}(M_i^p, M_i^g), & \text{if } \text{epoch} < t, \\ \mathcal{L}_i^{\text{MSE}}(M_i^p, M_i^g), & \text{if } \text{epoch} > t. \end{cases} \quad (14)$$

Overall Loss. To counteract category imbalance within counting datasets, which biases models toward indiscriminate counting, we propose a dual-phase loss for regions combined with uncertainty-based category count evaluation. The overall loss of FocalCount integrates both strategies:

$$\mathcal{L}_{\text{all}} = \frac{1}{n} \sum_{i=1}^n [U_C \mathcal{L}_i^D(M_i^p, M_i^g)], \quad (15)$$

4. Experimental Result

4.1. Datasets

FSC-147 [8] dataset is a class-agnostic counting dataset consisting of 6,135 images across 147 classes. It features

non-overlapping subsets and provides dot annotations for zero-shot counting.

CARPK [9] dataset includes 89,777 cars in 1,448 parking lot images, serving as an ideal benchmark for testing cross-dataset transferability.

SHANGHAI TECH [33] dataset is a crowd counting dataset with two parts: Part A (SHA) containing 482 images and Part B (SHB) containing 716 images. Each part contains 400 training images, with the remainder used for testing. Cross-part evaluations are challenging due to different data collection methods.

4.2. Evaluation Metrics.

We use mean absolute error (MAE) and root mean square error (RMSE) as evaluation metrics. MAE measures accuracy, while RMSE assesses robustness, following previous class-agnostic object counting methods [20].

4.3. Implementation Details

We evaluate our loss function on FSC-147 under both zero-shot and few-shot settings. Training uses a batch size of 32 and the AdamW [17] optimizer, starting with a learning rate of $1e-4$, decaying by a factor of 0.33 after 100 epochs. The training lasts for 300 epochs, with the first 50 epochs serving as the initial stage. Zero-shot training follows the CLIP-Count [11] baseline, while few-shot training follows the CACViT [29] baseline, with a weight decay of 0.05 and 10 warm-up epochs. All experiments, including ablation studies, are conducted on an NVIDIA RTX L40 GPU.

4.4. Comparison with State-of-the-Art Methods

Quantitative Results on FSC-147. Tab. 1 showcases FocalCount’s performance against state-of-the-art methods on FSC-147, particularly excelling in both few-shot and zero-shot settings on unseen datasets. In few-shot scenarios, while validation performance matches the baseline, incorporating Focal-MSE into CountX slightly boosts results and FocalCount achieves a 22-point reduction in test RMSE, enhancing its generalizability. This suggests a better handling of

| Scheme | Method | Venue | Shot | Val Set | | Test Set | | Avg | |
|----------------|------------------------------|-----------|------|--------------|--------------|--------------|---------------|--------------|--------------|
| | | | | MAE | RMSE | MAE | RMSE | MAE | RMSE |
| Reference-less | FamNet [22] | CVPR'21 | 0 | 32.15 | 98.75 | 32.27 | 131.46 | 32.21 | 115.11 |
| | RCC [8] | CVPR'22 | 0 | 17.49 | 58.81 | 17.12 | 104.53 | 17.31 | 81.67 |
| | CounTR [16] | BMVC'22 | 0 | 18.07 | 71.84 | 14.71 | 106.87 | 16.39 | 89.36 |
| | LOCA [3] | ICCV'23 | 0 | 17.43 | 54.96 | 16.22 | 103.96 | 16.83 | 79.46 |
| Few-shot | FamNet [22] | CVPR'21 | 1 | 26.05 | 77.01 | 26.76 | 110.95 | 26.41 | 93.98 |
| | FamNet [22] | CVPR'21 | 3 | 24.32 | 70.94 | 22.56 | 101.54 | 23.44 | 86.24 |
| | CFOCNet [31] | WACV'21 | 3 | 21.19 | 61.41 | 22.10 | 112.71 | 21.65 | 87.06 |
| | CounTR [16] | BMVC'22 | 3 | 13.13 | 49.83 | 11.95 | 91.23 | 12.54 | 70.53 |
| | PseCo [10] | CVPR'23 | 3 | 15.31 | 68.34 | 13.05 | 112.86 | 14.18 | 90.60 |
| | LOCA [3] | ICCV'23 | 3 | 10.24 | 32.56 | 10.97 | <u>56.97</u> | <u>10.61</u> | <u>44.77</u> |
| | CACViT [29] [†] | AAAI'24 | 3 | 11.41 | <u>39.75</u> | <u>10.47</u> | 66.24 | 10.94 | 52.99 |
| | CACViT + Ours | | 3 | <u>11.07</u> | 41.79 | 10.13 | 43.85 | 10.60 | 42.82 |
| Zero-shot | ZSC [30] | CVPR'23 | 0 | 26.93 | 88.63 | 22.09 | 115.17 | 24.51 | 101.90 |
| | VA-Count [34] | ECCV'24 | 0 | 17.87 | 73.22 | 17.88 | 129.31 | 17.87 | 101.26 |
| | CounTX [1] [†] | BMVC'23 | 0 | 18.32 | 63.21 | 18.47 | 106.15 | 18.39 | 84.68 |
| | CounTX + Ours | | 0 | 17.19 | 62.96 | 17.63 | 110.64 | 17.41 | 86.80 |
| | CLIP-Count [11] [†] | ACM MM'23 | 0 | 18.79 | <u>61.18</u> | <u>17.78</u> | <u>106.62</u> | 18.29 | <u>83.90</u> |
| | FocalCount (Ours) | | 0 | <u>18.57</u> | 61.02 | 17.60 | 102.74 | <u>18.08</u> | 81.88 |

Table 1. **Quantitative Comparison of the FocalCount Method with State-of-the-Art Methods on FSC-147.** † indicates models using the same backbone. The best and second-best results are highlighted in **bold** and underlined, respectively. Avg represents the average performance across the test and validation sets.

| Method | Venue | Shot | FSC → CARPK | |
|-------------------|-----------|------|--------------|--------------|
| | | | MAE | RMSE |
| FamNet [22] | CVPR'21 | 3 | 28.84 | 44.47 |
| BMNet [26] | CVPR'22 | 3 | 14.41 | 24.60 |
| BMNet+ [26] | CVPR'22 | 3 | 10.44 | 13.77 |
| RCC [8] | CVPR'22 | 0 | 21.38 | 26.61 |
| CLIP-Count [11] | ACM MM'23 | 0 | 13.59 | 18.30 |
| FocalCount (Ours) | | 0 | 12.74 | 15.33 |

Table 2. **Quantitative Comparison of FocalCount with State-of-the-Art Methods on CARPK.**

varied scenarios and reduced overfitting. In zero-shot settings, FocalCount outperforms the baseline on both validation and test sets, with a 4-point RMSE reduction, indicating fewer large errors and improved prediction stability. Although its MAE is slightly higher than VA-Count [34], the substantial 26-point drop in test RMSE highlights FocalCount’s robustness and superior generalization from learned representations to new data. The integration of Focal-MSE, though modest, underscores the potential for refining loss functions to improve counting accuracy, suggesting that even minor model adjustments can lead to significant performance enhancements.

Generalizability Evaluation on CARPK. To evaluate the cross-dataset generalizability of FocalCount, we train the model on FSC-147 and test it on CARPK without fine-tuning, following the protocol of previous class-agnostic

| Type | Method | SHB | | SHA | |
|----------|-------------------|--------------|--------------|---------------|---------------|
| | | MAE | RMSE | MAE | RMSE |
| Specific | MCNN [33] | 85.20 | 142.30 | 221.40 | 357.80 |
| | CrowdCLIP [13] | 69.60 | 80.70 | 217.00 | 322.70 |
| Generic | RCC [8] | 66.60 | 104.80 | 240.10 | 366.90 |
| | CLIP-Count [11] | 47.92 | 80.48 | 197.47 | 319.75 |
| | FocalCount (Ours) | 45.87 | 77.68 | 185.90 | 291.72 |

Table 3. **Cross-Dataset Evaluation on the SHANGHAI TECH Crowd Counting Dataset.** Generic models are trained on FSC-147, while specific models are trained on SHA.

counting approaches. As shown in Tab. 8, our method nearly matches the performance of few-shot methods on CARPK, achieving an MAE of 12.74 and an RMSE of 15.33. It outperforms other zero-shot methods, demonstrating robust generalizability.

Generalizability Evaluation on SHANGHAI TECH. To assess transferability and generalizability, we evaluate FocalCount on SHANGHAI TECH, following established protocols. As shown in Tab. 3, our model, trained exclusively on FSC-147, outperforms both methods transferred from crowd datasets and other generic models trained on FSC-147. It achieves lower error rates and demonstrates superior generalizability, indicating its robustness in handling highly variable crowd datasets.

| \mathcal{L}^{MSE} | \mathcal{L}^{ES} | U_C | Val Set | | Test Set | | Avg Set | |
|----------------------------|---------------------------|-------|--------------|--------------|--------------|---------------|--------------|--------------|
| | | | MAE | RMSE | MAE | RMSE | MAE | RMSE |
| ● | ○ | ○ | 18.78 | 62.23 | 18.29 | 105.74 | 18.54 | 83.98 |
| ○ | ● | ○ | 18.50 | 61.63 | 18.42 | 105.54 | 18.46 | 83.58 |
| ○ | ● | ● | 18.52 | 58.74 | 17.95 | 106.95 | 18.24 | 82.85 |
| ● | ● | ● | 18.57 | 61.02 | 17.60 | 102.74 | 18.08 | 81.88 |

Table 4. **Ablation Study on the Contribution of Each Component to the Final Results on FSC-147.** U_C denotes integrated uncertainty. Focal-MSE is applied during the initial training phase, while both MSE loss and U_C are utilized throughout the entire training process.

| Epoch | Val Set | | Test Set | | Avg Set | |
|-------|--------------|--------------|--------------|---------------|--------------|--------------|
| | MAE | RMSE | MAE | RMSE | MAE | RMSE |
| 10 | 19.35 | 65.83 | 18.94 | 107.61 | 19.14 | 86.72 |
| 20 | 18.57 | 61.02 | 17.60 | 102.74 | 18.08 | 81.88 |
| 30 | 18.58 | 63.96 | 17.09 | 102.09 | 17.84 | 83.03 |
| 40 | 18.88 | 63.87 | 18.39 | 106.73 | 18.64 | 85.30 |
| 50 | 18.83 | 63.19 | 18.39 | 106.58 | 18.61 | 84.88 |

Table 5. **Ablation Study on Different Pre-training Epochs.**

4.5. Ablation Study

Ablation Study on Various Factors. We conducted an ablation study to evaluate the contribution of each component in FocalCount, including Focal-MSE, MSE loss, ES loss, and multi-feature attribute uncertainty. Tab. 4 presents the results. Using MSE loss alone results in an MAE of 18.78 (first row), while using ES loss alone improves the MAE to 18.50 (second row). Adding uncertainty with ES loss further reduces the MAE to 18.24. Optimal performance is achieved when all components are integrated, showing that Focal-MSE effectively improves accuracy by addressing category-specific errors and data imbalance.

Ablation Study on Pre-training Epochs. To determine the optimal number of pre-training epochs, we conducted experiments whose results are presented in Tab. 5. Both 20 and 30 epochs produced strong results, but 20 epochs were selected as the optimal choice due to their superior RMSE, indicating greater robustness. The model trained with only 10 epochs performed the weakest, underscoring the importance of sufficient pre-training.

Ablation Study on Computational Cost Tab. 6 presents the computational times per batch for various configurations involving the loss functions \mathcal{L}^{MSE} , \mathcal{L}^{ES} , and uncertainty U_C . The results demonstrate that these configurations introduce only a modest increase in computational time. The highest recorded time is 2.24 milliseconds, slightly above the base time of 70 microseconds. This minimal increase indicates that the integration of enhanced loss functions and

uncertainty components does not significantly impact computational efficiency per batch. Consequently, our approach achieves improved model accuracy without incurring substantial computational overhead, ensuring efficient processing even with advanced algorithms.

| \mathcal{L}^{MSE} | \mathcal{L}^{ES} | U_C | Times | Avg Set | |
|----------------------------|---------------------------|-------|----------|--------------|--------------|
| | | | | MAE | RMSE |
| ● | ○ | ○ | 70.00 us | 18.54 | 83.98 |
| ○ | ● | ○ | 69.00 us | 18.46 | 83.58 |
| ● | ● | ○ | 84.00 us | 18.06 | 83.45 |
| ○ | ● | ● | 1.55 ms | 18.24 | 82.85 |
| ● | ○ | ● | 1.50 ms | 18.10 | 85.53 |
| ● | ● | ● | 2.24 ms | 18.08 | 81.88 |

Table 6. Ablation study on the contribution of each component and time to the final results on FSC-147 [8]. U_C denotes the integrated uncertainty. Focal-MSE is applied during the initial training phase, while MSE loss and U_C are employed throughout the entire process. Best results are highlighted in **bold**.

Tab. 7 compares different uncertainty methods. Each type of uncertainty leads to performance improvements, with the offset attribute U_2 providing the most significant enhancement. Combining all three uncertainties U_C yields the best performance, demonstrating that integrating attribute uncertainty improves robustness and addresses data imbalance.

Impact Analysis of Loss Functions. Fig. 6 shows the effect of different loss functions on model performance over the first 30 epochs, helping determine the optimal shift time in curriculum learning. During the first 10 epochs, ES loss (orange line) outperforms other loss functions, indicating the importance of early training in addressing error-prone regions. As training progresses, the advantage of ES loss diminishes, while MSE loss with uncertainty (orange line) consistently outperforms standard MSE loss in both MAE and RMSE. Within the first 20 epochs, Focal-MSE with uncertainty (red line) shows superior performance, surpassing the orange line. Ultimately, FocalCount (purple line) consistently outperforms standard MSE loss throughout training and surpasses all other loss functions.

| Metric | Val Set | | Test Set | | Avg Set | |
|--------|--------------|--------------|--------------|---------------|--------------|--------------|
| | MAE | RMSE | MAE | RMSE | MAE | RMSE |
| - | 18.78 | 62.23 | 18.29 | 105.74 | 18.53 | 83.99 |
| U_1 | 18.65 | 64.14 | 17.84 | 106.29 | 18.24 | 85.22 |
| U_2 | 18.22 | 64.08 | 17.77 | 106.99 | 17.99 | 85.53 |
| U_3 | 18.50 | 63.37 | 17.67 | 105.72 | 18.09 | 84.55 |
| U_C | 18.57 | 61.02 | 17.60 | 102.74 | 18.08 | 81.88 |

Table 7. **Ablation Study on Different Uncertainties.** U_1 , U_2 , U_3 , and U_C denote feature entropy, feature offset, feature certainty, and combined uncertainty, respectively.

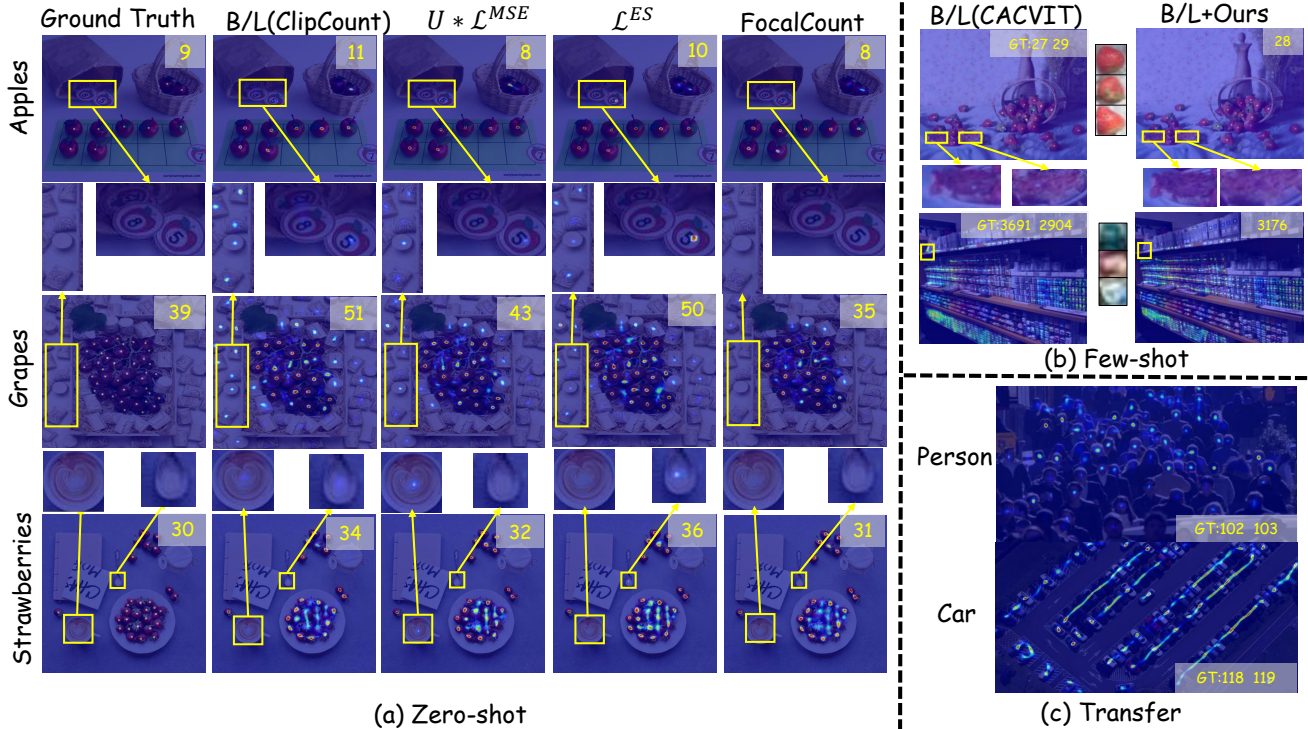


Figure 5. **Density Maps and Transfer Results in Zero-Shot and Few-Shot Settings.** (a) Density maps for different components in the zero-shot setting, with yellow boxes highlighting error-prone regions. (b) Comparison of density maps in the few-shot setting. (c) Transfer results from FSC-147 to SHANGHAI TECH and CARPK.

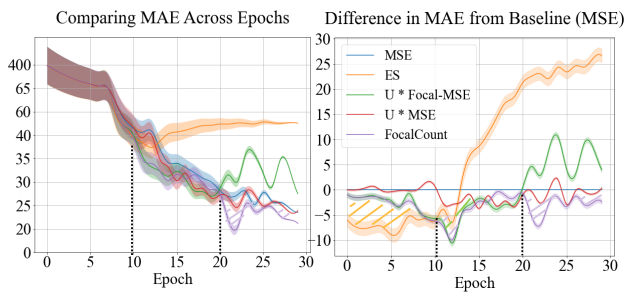


Figure 6. **Impact of Different Loss Functions on MAE during the First 30 Epochs.** The left panel shows the absolute impact, while the right panel compares the relative impact to the MSE loss. Y-axis intervals are adjusted for better visibility across a wide range of values.

Analysis of Specified Category Density Maps. Fig. 5(a) displays density maps under various settings, demonstrating the effectiveness of our method in reducing errors in non-specified categories. The first row shows improved differentiation between apple slices and whole apples, outperforming traditional reweighting techniques. The second row shows a significant reduction in miscounts of sharp-edged candles, outperforming both the baseline and slight

improvements over Focal-MSE. The third row, in a multi-category setting, illustrates effective differentiation between closely sized items like cups and spoons, outperforming both the baseline and partial Focal-MSE integration. Fig. 5(b) and (c) further illustrate our method’s efficacy in few-shot and transfer experiments, with reduced errors in challenging contexts. Our approach also demonstrates robustness in zero-shot and few-shot transfer, as shown in Fig. 5(c), where our model successfully adapts to unseen datasets such as SHANGHAI TECH and CARPK.

5. Conclusion

This paper introduces FocalCount, a novel method for addressing data imbalances in class-agnostic object counting by leveraging diverse feature attributes to accurately estimate object category counts within images. These estimates are used as weighted factors to correct class-count disparities. We also propose Focal-MSE, an enhanced loss function that refines traditional MSE by incorporating larger error gradients, thereby increasing sensitivity to errors in unspecified categories. By integrating curriculum learning, FocalCount improves quantity supervision and further enhances the model’s sensitivity to such errors. Extensive experiments on three object counting datasets, including

few-shot and zero-shot scenarios, validate the effectiveness of our approach. Notably, transfer tests on crowd and vehicle datasets demonstrate its robustness and generalizability. Future work will focus on advancing the model’s capabilities in category-discovery counting, extending beyond counting specific target objects.

Acknowledgments

This work was supported in part by the National Natural Science Foundation of China under Grant 62472332 and 62271361 and the Hubei Provincial Key Research and Development Program under Grant 2024BAB039.

References

- [1] Niki Amini-Naieni, Kiana Amini-Naieni, Tengda Han, and Andrew Zisserman. Open-world text-specified object counting. *arXiv:2306.01851*, 2023. 6
- [2] Carlos Arteta, Victor S. Lempitsky, and Andrew Zisserman. Counting in the wild. In *Proc. Eur. Conf. Comput. Vis.*, pages 483–498, 2016. 1
- [3] Nikola Djukic, Alan Lukezic, Vitjan Zavrtanik, and Matej Kristan. A low-shot object counting network with iterative prototype adaptation. In *Proc. IEEE/CVF Int. Conf. Comput. Vis.*, pages 18826–18835, 2023. 2, 3, 6
- [4] Zhipeng Du, Jiankang Deng, and Miaojing Shi. Domain-general crowd counting in unseen scenarios. In *Proc. AAAI Conf. Artif. Intell.*, pages 561–570, 2023. 2
- [5] Mark Everingham, Luc Van Gool, Christopher K. I. Williams, John M. Winn, and Andrew Zisserman. The pascal visual object classes (VOC) challenge. *Int. J. Comput. Vis.*, 88(2): 303–338, 2010. 5
- [6] Shenjian Gong, Shanshan Zhang, Jian Yang, Dengxin Dai, and Bernt Schiele. Class-agnostic object counting robust to intraclass diversity. In *Proc. Eur. Conf. Comput. Vis.*, pages 388–403, 2022. 2
- [7] Jiangpeng He and Fengqing Zhu. Gradient reweighting: Towards imbalanced class-incremental learning. In *Proc. IEEE/CVF Conf. Comput. Vis. Pattern Recognit.*, pages 16668–16677, 2024. 2
- [8] Michael A. Hobbey and Victor Prisacariu. Learning to count anything: Reference-less class-agnostic counting with weak supervision. *arXiv:2205.10203*, 2022. 5, 6, 7, 2
- [9] Meng-Ru Hsieh, Yen-Liang Lin, and Winston H. Hsu. Drone-based object counting by spatially regularized regional proposal network. In *Proc. IEEE/CVF Int. Conf. Comput. Vis.*, pages 4165–4173, 2017. 5, 2
- [10] Zhizhong Huang, Mingliang Dai, Yi Zhang, Junping Zhang, and Hongming Shan. Point, segment and count: A generalized framework for object counting. *arXiv:2311.12386*, 2023. 3, 6
- [11] Ruixiang Jiang, Lingbo Liu, and Changwen Chen. Clip-count: Towards text-guided zero-shot object counting. In *Proc. ACM Multimedia*, pages 4535–4545, 2023. 3, 5, 6
- [12] Seunggu Kang, WonJun Moon, Euiyeon Kim, and Jae-Pil Heo. Vlcounter: Text-aware visual representation for zero-shot object counting. In *Proc. AAAI Conf. Artif. Intell.*, pages 2714–2722, 2024. 3
- [13] Dingkan Liang, Jiahao Xie, Zhikang Zou, Xiaoqing Ye, Wei Xu, and Xiang Bai. Crowdclip: Unsupervised crowd counting via vision-language model. In *Proc. IEEE/CVF Conf. Comput. Vis. Pattern Recognit.*, pages 2893–2903, 2023. 6
- [14] Hui Lin, Zhiheng Ma, Xiaopeng Hong, Qinnan Shangguan, and Deyu Meng. Gramformer: Learning crowd counting via graph-modulated transformer. In *Proc. AAAI Conf. Artif. Intell.*, pages 3395–3403, 2024. 2
- [15] Tsung-Yi Lin, Priya Goyal, Ross B. Girshick, Kaiming He, and Piotr Dollár. Focal loss for dense object detection. *IEEE Trans. Pattern Anal. Mach. Intell.*, 42(2):318–327, 2020. 3
- [16] Chang Liu, Yujie Zhong, Andrew Zisserman, and Weidi Xie. Countr: Transformer-based generalised visual counting. In *Proc. Brit. Mach. Vis. Conf.*, page 370, 2022. 2, 6
- [17] Ilya Loshchilov and Frank Hutter. Decoupled weight decay regularization. In *Proc. Int. Conf. Learn. Represent.*, 2019. 5
- [18] Erika Lu, Weidi Xie, and Andrew Zisserman. Class-agnostic counting. In *Proc. Asian Conf. Comput. Vis.*, 2018. 2, 3
- [19] T. Nathan Mundhenk, Goran Konjevod, Wesam A. Sakla, and Kofi Boakye. A large contextual dataset for classification, detection and counting of cars with deep learning. In *Proc. Eur. Conf. Comput. Vis.*, pages 785–800, 2016. 1
- [20] Thanh Nguyen, Chau Pham, Khoi Nguyen, and Minh Hoai. Few-shot object counting and detection. In *Proc. Eur. Conf. Comput. Vis.*, pages 348–365, 2022. 2, 5
- [21] Shikai Qiu, Andres Potapczynski, Pavel Izmailov, and Andrew Gordon Wilson. Simple and fast group robustness by automatic feature reweighting. In *Int. Conf. Mach. Learn.*, pages 28448–28467, 2023. 2
- [22] Viresh Ranjan, Udbhav Sharma, Thu Nguyen, and Minh Hoai. Learning to count everything. In *Proc. IEEE/CVF Conf. Comput. Vis. Pattern Recognit.*, pages 3394–3403, 2021. 2, 3, 6
- [23] Viresh Ranjan, Udbhav Sharma, Thu Nguyen, and Minh Hoai. Learning to count everything. In *Proc. Asian Conf. Comput. Vis.*, pages 3121–3137, 2022. 2
- [24] Sudarshan Regmi, Bibek Panthi, Yifei Ming, Prashanna K Gyawali, Danail Stoyanov, and Binod Bhattarai. Reweightood: Loss reweighting for distance-based ood detection. In *Proc. IEEE/CVF Conf. Comput. Vis. Pattern Recognit.*, pages 131–141, 2024. 2
- [25] Deepak Babu Sam, Abhinav Agarwalla, Jimmy Joseph, Vishwanath A. Sindagi, R. Venkatesh Babu, and Vishal M. Patel. Completely self-supervised crowd counting via distribution matching. In *Proc. Eur. Conf. Comput. Vis.*, pages 186–204, 2022. 1
- [26] Min Shi, Hao Lu, Chen Feng, Chengxin Liu, and Zhiguo Cao. Represent, compare, and learn: A similarity-aware framework for class-agnostic counting. In *Proc. IEEE/CVF Conf. Comput. Vis. Pattern Recognit.*, pages 9519–9528, 2022. 2, 6
- [27] Aayush Kumar Tyagi, Chirag Mohapatra, Prasenjit Das, Govind Makharia, Lalita Mehra, Prathosh AP, and Mausam. Degpr: Deep guided posterior regularization for multi-class cell detection and counting. In *Proc. IEEE/CVF Conf. Comput. Vis. Pattern Recognit.*, pages 23913–23923, 2023. 1

- [28] Aäron van den Oord, Yazhe Li, and Oriol Vinyals. Representation learning with contrastive predictive coding. *arXiv:1807.03748*, 2018. [3](#)
- [29] Zhicheng Wang, Liwen Xiao, Zhiguo Cao, and Hao Lu. Vision transformer off-the-shelf: A surprising baseline for few-shot class-agnostic counting. In *Proc. AAAI Conf. Artif. Intell.*, pages 5832–5840, 2024. [2](#), [5](#), [6](#)
- [30] Jingyi Xu, Hieu Le, Vu Nguyen, Viresh Ranjan, and Dimitris Samaras. Zero-shot object counting. In *Proc. IEEE/CVF Conf. Comput. Vis. Pattern Recognit.*, pages 15548–15557, 2023. [3](#), [6](#)
- [31] Shuo-Diao Yang, Hung-Ting Su, Winston H. Hsu, and Wen-Chin Chen. Class-agnostic few-shot object counting. In *Proc. IEEE/CVF Winter Conf. Appl. Comput. Vis.*, pages 869–877, 2021. [2](#), [6](#)
- [32] Zhiyuan You, Kai Yang, Wenhan Luo, Xin Lu, Lei Cui, and Xinyi Le. Few-shot object counting with similarity-aware feature enhancement. In *Proc. IEEE/CVF Winter Conf. Appl. Comput. Vis.*, pages 6304–6313, 2023. [2](#)
- [33] Yingying Zhang, Desen Zhou, Siqin Chen, Shenghua Gao, and Yi Ma. Single-image crowd counting via multi-column convolutional neural network. In *Proc. IEEE/CVF Conf. Comput. Vis. Pattern Recognit.*, pages 589–597, 2016. [5](#), [6](#), [2](#)
- [34] Huilin Zhu, Jingling Yuan, Zhengwei Yang, Yu Guo, Zheng Wang, Xian Zhong, and Shengfeng He. Zero-shot object counting with good exemplars. In *Proc. Eur. Conf. Comput. Vis.*, 2024. [3](#), [6](#)

FocalCount: Towards Class-Count Imbalance in Class-Agnostic Counting

Supplementary Material

1. Evaluation Metrics

In accordance with previous class-agnostic object counting methods [20], we utilize the Mean Absolute Error (MAE) and Root Mean Square Error (RMSE) as evaluation metrics. MAE quantifies the average magnitude of prediction errors, thereby reflecting the model’s accuracy. In contrast, RMSE emphasizes larger errors, providing insights into the model’s robustness. The formal definitions of these metrics are presented in (16) and (17), where N denotes the number of images in the dataset, C_i represents the predicted count of objects in the i -th image, and C_i^{GT} is the corresponding ground-truth count.

$$\text{MAE} = \frac{1}{N} \sum_{i=1}^N |C_i - C_i^{\text{GT}}|, \quad (16)$$

$$\text{RMSE} = \sqrt{\frac{1}{N} \sum_{i=1}^N (C_i - C_i^{\text{GT}})^2}. \quad (17)$$

2. Ablation Study on Uncertainties

To evaluate the effectiveness of our uncertainty selection and combination strategies, we present the results in Tab. 8. Instead of using U_C , we applied a weighted average method to combine the uncertainties. Among the individual uncertainty components, U_2 demonstrated the most effective performance. However, pairwise combinations did not yield improvements, likely due to interference between uncertainties. Although integrating all three uncertainties achieved competitive performance, it did not surpass the effectiveness of using a single uncertainty component, as interference persisted. In contrast, our approach leverages a Dirichlet distribution to combine uncertainties, achieving optimal results and outperforming methods that rely solely on individual uncertainty components. This underscores the efficacy and necessity of using a Dirichlet distribution for effectively managing combined uncertainties.

3. Analysis of Density Maps

To demonstrate the performance of our method across zero-shot, transfer, and few-shot scenarios, we present Fig. 7, Fig. 8, and Fig. 9. These figures illustrate our model’s ability to accurately distinguish between different object categories in specified density maps, highlighting its robustness and adaptability under various testing conditions.

Fig. 7 shows density maps resulting from transferring our model directly from FSC-147 [8] to SHANGHAITECH [33]

| U_1 | U_2 | U_3 | U_C | Val Set | | Test Set | | Avg Set | |
|-------|-------|-------|-------|--------------|--------------|--------------|---------------|--------------|--------------|
| | | | | MAE | RMSE | MAE | RMSE | MAE | RMSE |
| ● | ○ | ○ | ○ | 18.65 | 64.14 | 17.84 | 106.29 | 18.24 | 85.22 |
| ○ | ● | ○ | ○ | 18.22 | 64.08 | 17.77 | 106.99 | 17.99 | 85.53 |
| ○ | ○ | ● | ○ | 18.50 | 63.37 | 17.67 | 105.72 | 18.09 | 84.55 |
| ○ | ○ | ○ | ● | 19.17 | 69.07 | 18.62 | 110.01 | 18.89 | 89.54 |
| ● | ○ | ● | ○ | 18.99 | 67.39 | 18.51 | 114.98 | 18.75 | 91.18 |
| ● | ● | ○ | ○ | 18.90 | 68.06 | 18.24 | 112.80 | 18.57 | 90.43 |
| ● | ● | ● | ○ | 18.55 | 66.27 | 18.13 | 110.11 | 18.34 | 88.19 |
| ● | ● | ● | ● | 18.57 | 61.02 | 17.60 | 102.74 | 18.08 | 81.88 |

Table 8. Ablation Study on Different Uncertainties. U_1, U_2, U_3 , and U_C denote feature entropy, feature offset, feature certainty, and combined uncertainty, respectively. The best results are highlighted in bold.

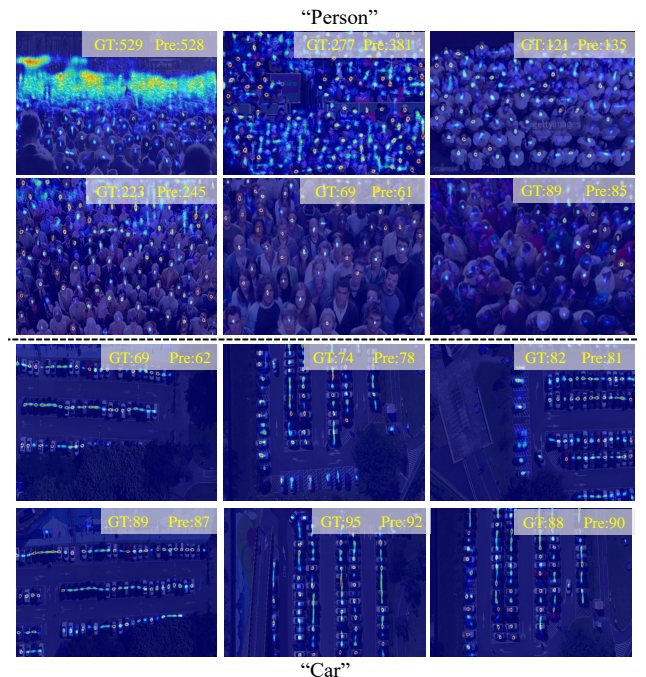


Figure 7. Density Maps of Transfer to Human and Vehicle Categories.

and CARPK [9] without additional training. Despite the challenges posed by dense crowd scenarios, our transfer experiments demonstrate the method’s effectiveness, particularly in the vehicle dataset, which exhibited even fewer errors.

Fig. 8 highlights the model’s capability to distinguish and quantify different object categories in a zero-shot setting. This figure demonstrates the model’s proficiency in

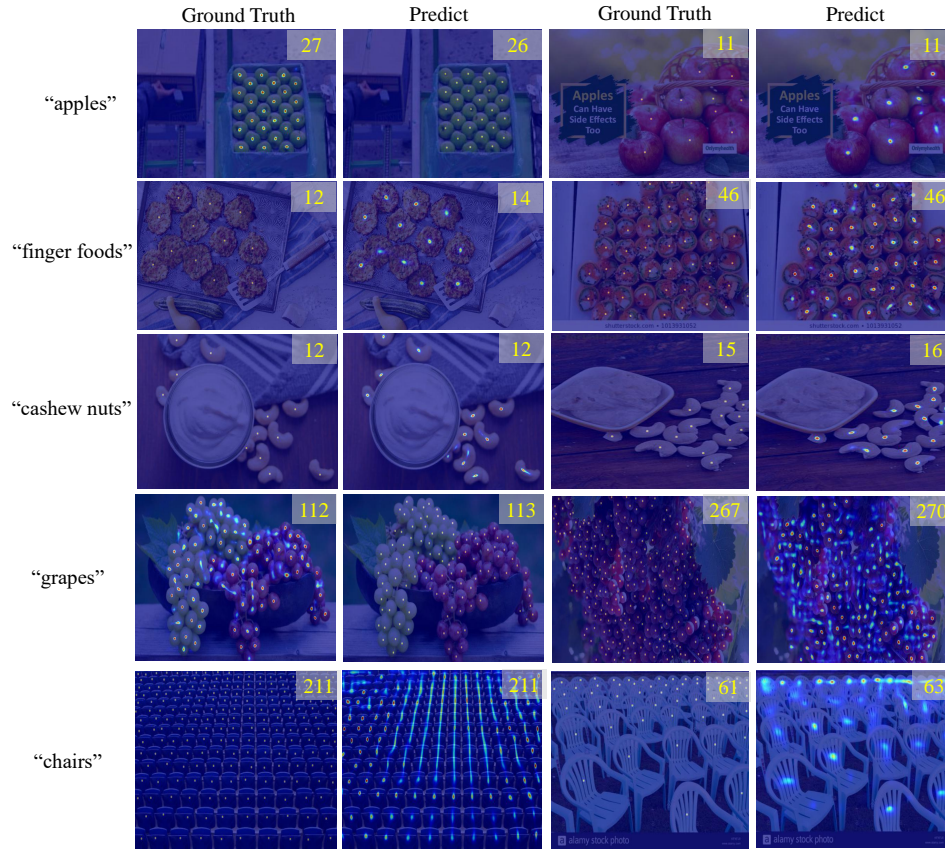


Figure 8. Density Maps of Specified Categories in the Zero-Shot Setting.

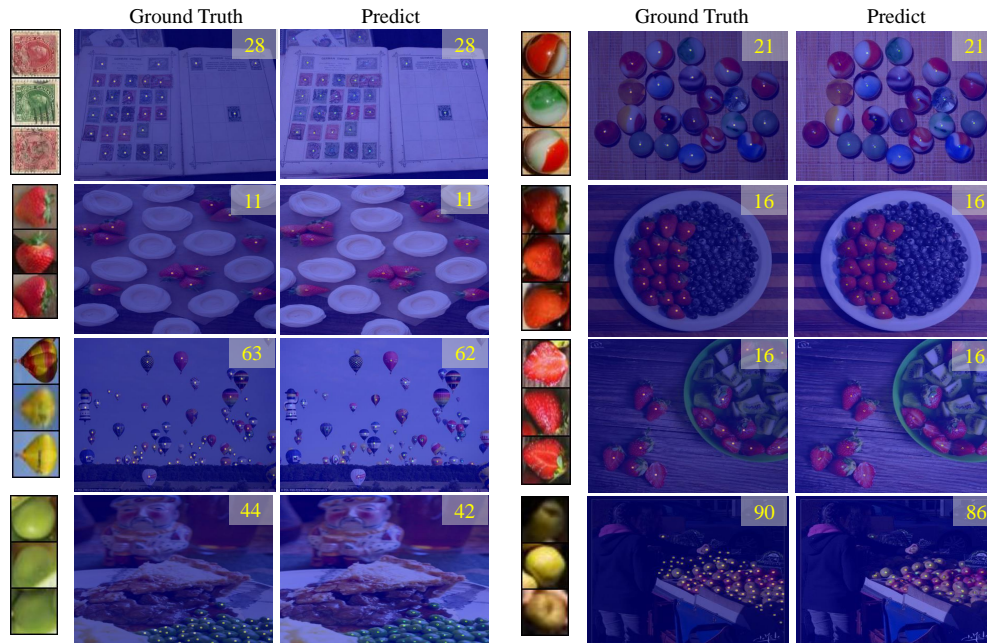


Figure 9. Density Maps of Specified Categories in the Few-Shot Setting.

handling objects with diverse densities and configurations by comparing predicted counts against ground truths across various categories, including apples, finger foods, cashew nuts, grapes, and chairs. The results indicate the model's potential for accurate object recognition and counting without prior category-specific training, a crucial capability for real-world applications where new object types frequently emerge.

Fig. 9 showcases the model's performance in a few-shot setting, where it accurately identifies and counts different categories within images. This underscores the model's precision in distinguishing between various objects under limited training scenarios, ranging from everyday items like plates and fruits to more complex scenes involving balloons and marketplaces. The close alignment between predicted counts and ground truths across diverse scenes underscores the effectiveness of the few-shot learning approach in handling a variety of visual contexts with minimal prior data exposure.